Formation of Sn-induced nanowires on Si(557)

M. Jäger[1], H. Pfnür[1], M. Fanciulli[2,3], A.P. Weber[2,3], J.H. Dil[2,3], C. Tegenkamp[*,1,4]

[1] Institut für Festkörperphysik, Leibniz Universität Hannover, Appelstrasse 2, 30167 Hannover, Germany
[2] Photon Science Division, Paul Scherrer Institut, 5232 Villigen PSI, Switzerland
[3] Institute of Physics, École Polytechnique Fédérale de Lausanne, 1015 Lausanne, Switzerland
[4] Institut für Physik, Technische Universität Chemnitz, Reichenhainer Str. 70, 09126 Chemnitz, Germany

Key words: Sn nanowires, vicinal Si(111), scanning tunneling microscopy

* Corresponding author: e-mail christoph.tegenkamp@physik.tu-chemnitz.de

In this study we analyzed the growth of Sn on Si(557) surfaces by means of scanning tunneling microscopy, low energy electron diffraction and angle resolved photoemission. Depending on the Sn submonolayer coverage, various Sn-nanowires were identified. For Sn-coverages above 0.5 ML, $(\sqrt{3}\times\sqrt{3})$- and $(2\sqrt{3}\times 2\sqrt{3})$-reconstructions were found. In particular, these phases cover extended (111)-areas, thus leading to an inhomogeneous refacetting of the Si(557) surface. The (223)-facets between the mini-(111) terraces reveal structures, which resemble a $\times 2$ reconstruction along edges. The initial step structure of the Si(557) surface is maintained for Sn-coverages below 0.5 ML, showing the α-Sn phase on 3 nm wide (111)-terraces. In contrast to the 2D Mott state of α-Sn/Si(111), this confinement seems to quench the correlated electronic phase yielding metallic surface states at 40 K, in accordance with photoemission.

1 Introduction Nanowires grown by self-assembly on surfaces were shown to provide a perfect template to study fundamental ground state properties of one-dimensional systems. Moreover, they also appear to be interesting candidates for getting a deep insight into the transient of a phase transition or dynamics of solitons, as impressively demonstrated for In/Si(111) [1,2,3].

Driven by these fascinating effects, other atomic wire systems were synthesized with different adsorbates mainly deposited on silicon substrates in which the surface states are well decoupled from the bulk states. For instance, rare-earth or transition metals form partially embedded silicide wires [4,5,6,7]. Submonolayer coverages of Au on vicinal Si(111) exchange with Si-surface atoms forming long range ordered atomic chains with metallic Rashba-split surface bands [8,9]. On the other hand, metals like Ag or Pb evaporated on Si(557) do not intermix with silicon but form densely-packed layers covalently bonded to the top layer of the substrate [10,11,12]. For Ag/Si(557) the surface facet structure of the bare substrate is preserved upon adsorption, consisting of triple steps with (111)-oriented areas of ~ 4 nm in width [10]. In contrast, the deposition of Pb results in formation of a different surface orientation, i.e., the Pb nanowires grow on (223) facets with a terrace width of 1.55 nm. The Pb/Si(557) was shown to host a spin-orbit density wave [13] as a consequence of the interplay between spin-orbit coupling (SOC), the band filling factors and interwire distance. Also for Pb/Si(553) giant spin-orbit splitting was reported [12].

A potential candidate for nanowires revealing electronic correlation effects might be Sn/Si(557). Recently, it was shown that the two-dimensional analog, i.e. the α-Sn phase on Si(111), gives rise to a Mott phase which is to some extent influenced by SOC, even though the SOC strength and the resulting Rashba-splitting is significantly smaller compared to the isoelectronic Pb. Electronically, the Mott phase gives rise to a $(2\sqrt{3}\times\sqrt{3})$ unit cell due to the antiferromagnetic ordering between adjacent rows of the $(\sqrt{3}\times\sqrt{3})$-structure [14,15].

The targeted manipulation of Mott-systems arouse a lot of interest. For instance, doping leads to various phases like high-temperature superconductivity [16], charge-transfer insulators [17], or robust metallic states [18]. For α-Sn on Si(111) a metallic quasi-particle state was found within the Mott gap, if the system is modified by means of the acceptor concentration of the Si substrate [19]. In this con-

text, the growth of Mott-phases of finite widths is interesting and was not considered before. Step edges may provide binding sites with electronic properties different from the flat surface, leading to partially ionized atoms. In the case of Ag/Si(557), this results in doping of electrons to the nanowires [20]. In addition, a refacetting similar to Pb/Si(557) implies a terrace width of approximately the same size as one unit cell of the low-temperature $(2\sqrt{3} \times \sqrt{3})$ structure and might suppress the formation of it.

In this paper we analyze the growth of Sn on Si(557) in order to elucidate the possibility to form defined nanowires. By choosing different coverages we were able to identify three distinct phases by means of STM and LEED. Deposition of more than 0.5 ML of Sn leads to the formation of the high coverage $(2\sqrt{3} \times 2\sqrt{3})$ phase on (111) terraces that destabilizes the triple steps, resulting in a local (223) orientation. If the $(2\sqrt{3} \times 2\sqrt{3})$ stripes grow larger, step bunching occurs, eventually resulting in a surface covered by large (111) terraces. Only for lower Sn coverages, ordered stripes of Sn- wires with $(\sqrt{3} \times \sqrt{3})$ symmetry separated by triple steps were found. As observed by ARPES, this confinement destroys the insulating nature of the spin-split ground state, pointing towards a finite-size induced quenching of the Mott state.

2 Experimental details Well oriented surfaces of phosphorous-doped Si(557) samples (< 5 mΩcm) were prepared by degassing at 500 °C for several hours and repeated flash annealing to 1150 °C until a sharp (7×7) reconstruction and step-train patterns were seen in optical LEED. In order to prepare the nanowires, different amounts of Sn, i.e. 0.4 monolayer (ML$= 7.8 \times 10^{14}$ cm^{-2}, defined with respect to Si(111)), 0.6 ML and 0.9 ML, were deposited at a rate of around 0.02 ML/min on the surface. During evaporation, the substrate is kept at a temperature of 570$\pm$20 °C. The samples were investigated by means of low energy electron diffraction (LEED), scanning tunneling microscopy (STM) and angle-resolved photoemission (ARPES). LEED and STM measurements were performed at room temperature. ARPES measurements were done at the COPHEE endstation at the SIS beamline of the Swiss Light Source, using right circularly (C^+) and linearly (p) polarized light with a photon energy of 44 eV. The photoemission experiments were carried out with an energy and angle resolution of 25 meV and 0.5° at low temperatures (40 K), well below the phase transition temperature of ~ 70 K for the α-Sn phase on Si(111).

3 Results and Discussion Evaporation of submonolayer coverages of Sn on vicinal Si(557) results in the formation of three distinct phases. Fig. 1 presents large scale STM images and LEED patterns with different Sn coverages of 0.4 ML (panel a,d), 0.6 ML (b,e) and 0.9 ML (c,f). For the lowest Sn coverage of 0.4 ML the former step structure of the Si(557) surface is preserved as deduced from the spot splitting of $\Delta k = 0.1$ Å^{-1} around the (1×1) diffraction spots in LEED along the $[11\bar{2}]$-direction. In addition, a weak $\times 2$ streak is visible as well as pronounced $(\sqrt{3} \times \sqrt{3})$ diffraction spots (marked by red hexagons). The homogeneously stepped surface can be confirmed by STM, showing a nanowire-like structure. A slight azimuthal miscut restricts the length of the wires to approximately 200 nm.

Increasing the Sn coverage to 0.6 ML, the structure of the surface changes entirely (cf. Figs. 1b,e). Sharp diffraction spots seen in LEED between the (1×1) spots in the $[1\bar{1}0]$-direction reveal spot splitting of a homogeneously stepped (223) surface orientation, similar to the adsorption of Pb/Si(557) [13]. Again $(\sqrt{3} \times \sqrt{3})$ diffraction spots are visible, but in addition also diffraction spots originating from a $(2\sqrt{3} \times 2\sqrt{3})$ reconstruction are present. In consequence of the formation of (223) facets, the initial (557)-oriented surface builds up larger (111)-areas in order to maintain the average inclination. This local refacetting shows up in STM by the formation of bundle-like structures. Their width is around 20 nm and, compared to the low coverage phase, the length decreases down to 100 nm.

Covering the Si(557) surface with an even larger Sn coverage, i.e., 0.9 ML, the diffraction spots coming from (223) orientation vanish in LEED (Fig. 1f). The $(2\sqrt{3} \times 2\sqrt{3})$ reconstruction becomes more intense and a streaky feature appears at the $\times 2$ positions. However, the appearance is quite similar to the intermediate coverage phase. The nanowire bundles still exhibit approximately the same size, but now the structure of these bundles can be resolved more clearly even in a large scale STM picture shown in Fig. 1c). They seem to consist of few nanowires which appear to be much wider than with less coverage. In the following, the atomic structure of the nanowires at the different Sn coverages will be explained in more detail.

3.1 Intermediate and high coverage nanowires, Sn >0.5 ML The α-Sn phase on Si(111) comprises ideally 1/3 ML. For higher coverages a mixture of $(\sqrt{3} \times \sqrt{3})$ and $(2\sqrt{3} \times 2\sqrt{3})$ domains is expected, in agreement with the phase diagram for Sn/Si(111) [21]. The latter phase has a nominal Sn coverage of around 1.2 ML [22]. Although the atomic structure is still under debate, latest results favor the model by Toernevik et al. containing 14 Sn atoms per unit cell arranged in a double layer, with its top layer comprising of four atoms [23,24] .

The (111)-terrace size of the clean and homogeneously stepped Si(557) surface is 1.9 nm, thus large enough to form a $(2\sqrt{3} \times 2\sqrt{3})$ unit cell. Obviously, a different scenario is energetically favored, as seen in Fig. 2 for 0.6 ML Sn. The double layered $(2\sqrt{3} \times 2\sqrt{3})$ structure destabilizes the step structure of the Si(557) surface and increases the width of the (111) terraces, as seen by STM. The (111) terraces are between 5 and 20 nm wide and, indeed, a phase mixture of $(\sqrt{3} \times \sqrt{3})$ and $(2\sqrt{3} \times 2\sqrt{3})$ reconstructions is observed on them (Fig. 2(b)). As a consequence, steeper areas are formed resembling locally a (223)-facet structure.

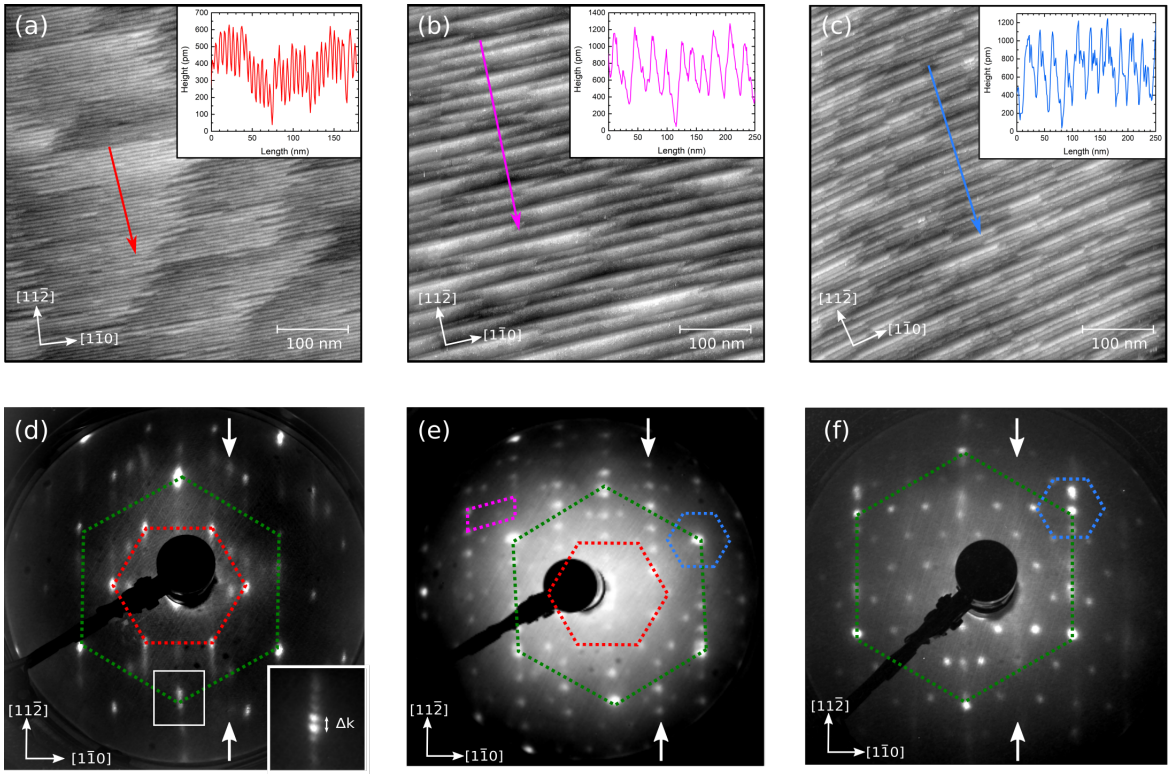

Figure 1 (a–c) STM images of Sn coverage dependent phases on Si(557): (a) 0.4 ML (tunneling condition -1 V, 1 nA), (b) 0.6 ML (1 V, 0.1 nA) and (c) 0.9 ML (-2 V, 0.1 nA). Arrows indicate the directions of the linescans shown in the insets. (d–f) LEED images taken at electron energies around 80 eV corresponding to the STM pictures shown above. Dashed lines indicate the (1×1) (green), $(\sqrt{3} \times \sqrt{3})$ (red), $\times 2$ (purple) and $(2\sqrt{3} \times 2\sqrt{3})$ (blue) unit cells in reciprocal space, white arrows show the $\times 2$ positions. Inset in (d): Enlarged area around the (1×1) spot highlighting the spot splitting Δk across the step direction of the Si(557).

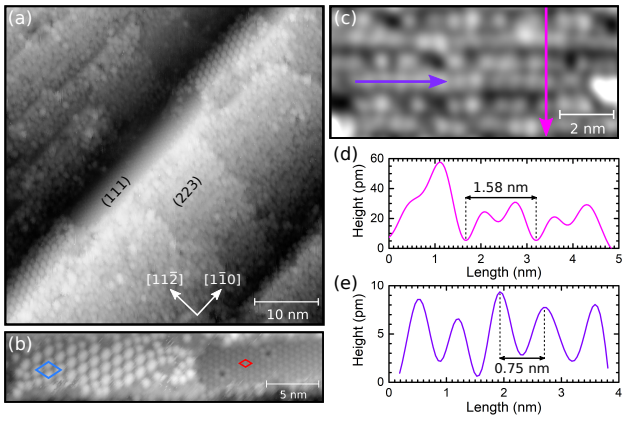

Figure 2 (a) STM image (-1 V, 0.1 nA) of the 0.6 ML Sn phase on Si(557). (b) Enlarged image of the coexisting $(\sqrt{3}\times\sqrt{3})$ and $(2\sqrt{3}\times 2\sqrt{3})$ structure on the (111) terraces taken at (-1 V, 80 pA), unit cells are indicated in red and blue, respectively. (c) Enlarged image of the (223) oriented part (-1 V, 50 pA). The arrows indicate the directions where the line scans, shown in (d) and (e), were taken.

The (223) oriented parts consist of small steps with a distance of 1.58 nm, as seen in Fig. 2(c) and (d). On each step two rows of Sn-atoms can be resolved. Along the chains the tin atoms have a spacing of $2a_0 = 0.75$ nm (see Fig. 1(e)), corresponding to the sharp $\times 2$ phase seen in LEED (cf. Fig. 1e, purple unit cell). This reconstruction is concomitant with a step-step correlation within the (223)-facet structure giving rise to the sharp diffraction spots and has been seen for other systems as well [25,26]. As obvious from Fig. 2(c), these atomic chains are not as free of defects as other nanowire systems on vicinal substrates (e.g. cf. with Pb/Si(557) [13]). In order to improve the long-ranged order along the steps, additional 0.1 ML of tin were added with the substrate temperature kept at 550 °C. However, the additional Sn tends to accumulate only on the (111) terraces, not on the (223) facets, resulting in even larger $(2\sqrt{3} \times 2\sqrt{3})$ domains on the (111) terraces, and eventually covering the entire terrace when the Sn coverage is increased even more.

Above a Sn coverage of $\approx 2/3$ ML the high coverage nanowire phase represents the majority. The wider (111) terraces are completely covered by a $(2\sqrt{3} \times 2\sqrt{3})$ recon-

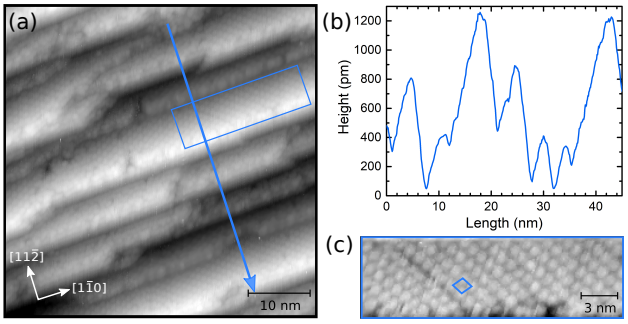

Figure 3 (a) STM image of the 0.9 ML Sn phase on Si(557). Blue arrow indicates the direction of the linescan shown in (b). (c) Enlarged image of the $(2\sqrt{3} \times 2\sqrt{3})$ structure on the terraces. The unit cell is indicated in blue. Images were taken at (2 V, 60 pA)

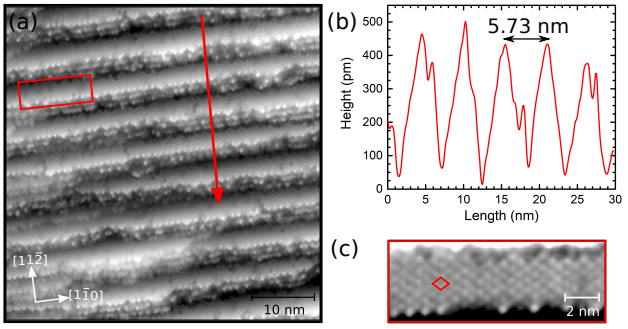

Figure 4 (a) STM image of the 0.4 ML Sn phase on Si(557). Red arrow indicates the direction of the linescan shown in (b). (c) Enlarged image of the $(\sqrt{3} \times \sqrt{3})$ structure on the terraces. The unit cell is indicated in red. Images were taken at (1 V, 1 nA)

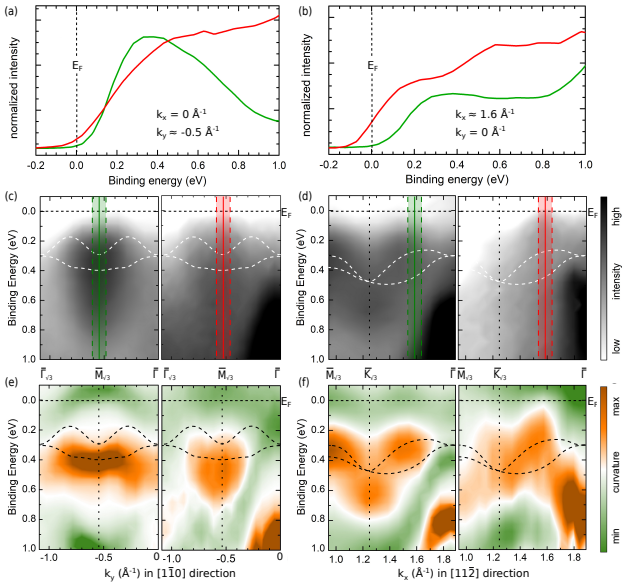

Figure 5 (a), (b) EDCs for surface states along the $[1\bar{1}0]$-direction (at $k_y \approx -0.5$ Å, $k_x = 0$ Å) and $[11\bar{2}]$-direction (at $k_x \approx 1.6$ Å, $k_y = 0$ Å), respectively. Red lines correspond to low coverage Sn/Si(557) nanowires, green lines are from α-Sn/Si(111) and are shown for comparison. c) Band maps of the Mott-state along the $[1\bar{1}0]$-direction for α-Sn phase on Si(111) (left, 90 eV photon energy, 40 K) and Si(557) (right, 44 eV photon energy, 40 K). d) Band maps like in panel c) but along the $[11\bar{2}]$-direction. (e), (f) Curvature maps of (c) and (d) to highlight details of the band structure. The Sn/Si(111) data were reproduced from data shown in Ref. [15]. The dashed lines refer to band structure calculations for Sn/Si(111) [29, 15].

struction and further excess Sn would have to accumulate on the local (223) orientated parts. Although these small terraces provide a width suitable for the formation of a $(2\sqrt{3} \times 2\sqrt{3})$ unit cell, larger domains are favored and further Sn deposition leads to step bunching, resulting in a surface dominated by large (111) terraces (Fig. 3a). They are entirely covered by a $(2\sqrt{3} \times 2\sqrt{3})$ reconstruction. The terrace widths appear to be quite irregular, but they are usually a multiple of 1.33 nm, which is the lattice constant of the Sn reconstruction.

Summarizing this part, the formation of extended α-Sn phases, which may undergo a metal to insulator transition at low temperatures and formation of $(2\sqrt{3} \times 2\sqrt{3})$ reconstructions on (111) areas, drive the refacetting of the initial Si(557) orientation. This is in contrast to Pb/Si(557), where the nesting condition found for Pb/Si(557) favors the formation of a (223) facet structure with a well defined atomic Pb-induced reconstruction [27, 13].

3.2 Low coverage nanowires (Sn <0.5 ML): a pseudo-gapped Mott state? Only in the low Sn-coverage regime the initial surface structure of Si(557) is preserved. The spacing between two adjacent terraces is 5.73 nm (cf. Fig. 4(b)) which corresponds to the spot splitting observed by LEED. STM measurements, shown in Fig. 4, reveal that the surface structure consists of approximately 3 nm wide (111) terraces covered with a $(\sqrt{3} \times \sqrt{3})$-Sn structure separated by triple steps, similar to Ag/Si(557) [10]. The $(\sqrt{3} \times \sqrt{3})$-Sn reconstruction on the mini-(111) terraces is well-known for 0.3 ML Sn coverage on Si(111) surface [28, 22]. The $\times 2$-periodicity originates from Si-dimers along the step edges. The edge roughness is mainly a result of the zig-zag edges of the Sn-reconstruction along the $[1\bar{1}0]$-direction.

This phase is in particular interesting for electronic investigations. Compared to higher coverage phases, only the 0.4 ML Sn-phase on Si(557) results in the formation of an homogeneously stepped structure with defined 3 nm wide stripes hosting a α-Sn reconstruction. As mentioned, the α-Sn/Si(111) system is a prototype system for a metal-insulator transition at $T_c \approx 70\ K$ [30]. Therefore, this phase is suitable to probe finite-size effects for a surface

Mott system. As shown in Fig. 5 a) and b) energy distribution curves (EDC) were taken at two different points in k-space at 40 K. Along the $[1\bar{1}0]$-direction, the spectral weight at E_F is strongly suppressed for both the flat (green line) and vicinal (red line) surface. On the other hand, whereas along the $[11\bar{2}]$-direction the surface state on the flat surface shows a clear Mott gap [15], a considerable intensity is found at E_F for the same state on the vicinal surface. The band maps, which correspond to the EDCs, are shown in Fig. 5(c) and (d), as well as curvature plots ((e) and (f)). The latter shows the dispersion of the surface state in more detail. The calculated band structure of α-Sn/Si(111) [29] is superimposed in order to highlight the alteration of the surface state in case of the vicinal substrate, especially in the $[11\bar{2}]$-direction. Furthermore, the intensity of the Sn/Si(557) surface state appears to be weaker than for Sn/Si(111). Since a lack of sample quality is excluded by means of LEED, which was done prior to the ARPES measurements, the decrease in intensity is attributed to the confined size of the α-Sn reconstruction, and the presence of stepped areas in between. Apparently, the Sn/Si(557) in this coverage regime resembles a pseudo-gapped Mott state.

Recently, Ming et al. [19] succeeded in doping the α-Sn/Si(111) phase via changing the substrate's doping level. Upon hole doping, STS measurements show the development of a quasi-particle state inside the Mott-insulating gap of the system. In the case considered here, doping might be induced via step edges. As already known for Ag/Si(557), excess atoms adsorbed on step edges leads to electron-doping of the system. Along the step edges of these Sn nanowires, silicon dimers are present (cf. with $\times 2$ streaks seen in LEED, Fig. 1(d)) as well as tin atoms. This may lead to an additional state close to E_F, that is seen in ARPES in superposition with the insulating state originating from the α-Sn phase. Alternatively, we should consider the finite width of the α-Sn nanowires, which is comparable to the coherence lengths of the Mott state which can be approximately calculated via $\xi = 2\hbar v_F/\pi\Delta$, where Δ is the energy gap and v_F the Fermi velocity of the electrons [31]. From our ARPES data we can estimate $\xi \approx 2-3\,nm$, thus the finite width along the $[11\bar{2}]$-direction quenches the Mott state in this direction resulting in a pseudo-gapped Mott state in α-Sn nanowires.

4 Summary and Conclusion In summary, we studied in detail the growth of Sn on Si(557) substrates. In total we were able to identify three different stable phases. For coverages needed to form the α-Sn phase on Si(111) the initial surface facet structure is maintained. Increasing of the Sn coverage leads to $(2\sqrt{3}\times 2\sqrt{3})$ domains, that tend to develop on large (111) terraces. That first results in locally (223) oriented parts separated by wider (111) terraces, and eventually the whole surface is covered with (111) terraces due to step bunching.

For coverages of 0.4 ML Sn we found a homogeneously stepped array of α-Sn nanowires. ARPES measurements on this phase below T_c for the Mott transition on Sn/Si(111) clearly showed a metallic surface state along the $[11\bar{2}]$-direction. Both, doping of the Mott phase due to the presence of edges or the finite width the wires seem to be responsible for the quenched Mott-gap along the $[11\bar{2}]$-direction.

Acknowledgement
The final support by the Deutsche Forschungsgemeinschaft through project Te386/10-2 of the FOR1700 Research Unit is gratefully acknowledged.

References

[1] T.-H. Kim, S. Cheon, H. W. Yeom, *Nat. Phys.* **2017**, *13*, 444.
[2] T. Frigge, B. Hafke, T. Witte, B. Krenzer, C. Streubühr, A. Samad Syed, V. Mikšić Trontl, I. Avigo, P. Zhou, M. Ligges, D. von der Linde, U. Bovensiepen, M. Horn-von Hoegen, S. Wippermann, A. Lücke, S. Sanna, U. Gerstmann, W. G. Schmidt, *Nature* **2017**, *544*, 207.
[3] C. W. Nicholson, A. Lücke, W. G. Schmidt, M. Puppin, L. Rettig, R. Ernstorfer, M. Wolf, *Science* **2018**, *362*, 821.
[4] H. W. Yeom, Y. K. Kim, E. Y. Lee, K.-D. Ryang, P. G. Kang, *Phys. Rev. Lett.* **2005**, *95*, 205504.
[5] V. Iancu, P. R. C. Kent, S. Hus, H. Hu, C. G. Zeng, H. H. Weitering, *J. Phys.: Condens. Matter* **2012** *25*, 014011.
[6] S. Appelfeller, M. Franz, H.-F. Jirschik, J. Große, M. Dähne, *New J. Phys.* **2016**, *18*, 113005.
[7] I. Miccoli, F. Edler, H. Pfnür, S. Appelfeller, M. Dähne, K. Holtgrewe, S. Sanna, W. G. Schmidt, C. Tegenkamp, *Phys. Rev. B* **2016**, *93*, 125412.
[8] J. N. Crain, J. L. McChesney, F. Zheng, M. C. Gallagher, P. C. Snijders, M. Bissen, C. Gundelach, S. C. Erwin, F. J. Himpsel, *Phys. Rev. B* **2004**, *69*, 125401.
[9] B. Hafke, T. Frigge, T. Witte, B. Krenzer, J. Aulbach, J. Schäfer, R. Claessen, S. C. Erwin, M. Horn-von Hoegen, *Phys. Rev. B* **2016**, *94*, 161403.
[10] U. Krieg, C. Brand, C. Tegenkamp, H. Pfnür, *J. Phys.: Condens. Matter* **2013**, *25*, 014013.
[11] M. Czubanowski, A. Schuster, S. Akbari, H. Pfnür, C. Tegenkamp, *New J. Phys.* **2007**, *9*, 338.
[12] M. Kopciuszyński, M. Krawiec, R. Zdyb, M. Jałochowski, *Sci. Rep.* **2017**, *7*, 46215.
[13] C. Brand, H. Pfnür, G. Landolt, S. Muff, J. H. Dil, T. Das, C. Tegenkamp, *Nat. Comm.* **2015**, *6*, 8118.
[14] G. Li, P. Höpfner, J. Schäfer, C. Blumenstein, S. Meyer, A. Bostwick, E. Rotenberg, R. Claessen, W. Hanke, *Nat. Comm.* **2013**, *4*, 1620.
[15] M. Jäger, C. Brand, A. P. Weber, M. Fanciulli, J. H. Dil, H. Pfnür, C. Tegenkamp, *Phys. Rev. B* **2018**, *98*, 165422.
[16] A. Damascelli, Z. Hussain, Z.-X. Shen, *Rev. Mod. Phys.* **2003**, *75*, 473.
[17] G. Amow, N. Raju, J. Greedan, *J. Solid State Chem.* **2000**, *155*, 177.
[18] G. Affeldt, T. Hogan, C. L. Smallwood, T. Das, J. D. Denlinger, S. D. Wilson, A. Vishwanath, A. Lanzara, *Phys. Rev. B* **2017**, *95*, 235151.

[19] F. Ming, S. Johnston, D. Mulugeta, T. S. Smith, P. Vilmercati, G. Lee, T. A. Maier, P. C. Snijders, H. H. Weitering, *Phys. Rev. Lett.* **2017**, *119*, 266802.
[20] U. Krieg, T. Lichtenstein, C. Brand, C. Tegenkamp, H. Pfnür, *New J. Phys.* **2015** *17*, 043062.
[21] T. Ichikawa, *Surf. Sci.* **1984**, *140*, 37.
[22] C. Törnevik, M. Göthelid, M. Hammar, U. Karlsson, N. Nilsson, S. Flodström, C. Wigren, M. Östling, *Surf. Sci.* **1994**, *314*, 179.
[23] S. Yi, F. Ming, Y.-T. Huang, T. S. Smith, X. Peng, W. Tu, D. Mulugeta, R. D. Diehl, P. C. Snijders, J.-H. Cho, H. H. Weitering, *Phys. Rev. B* **2018**, *97*, 195402.
[24] C. Törnevik, M. Hammar, N. G. Nilsson, S. A. Flodström, *Phys. Rev. B* **1991**, *44*, 13144.
[25] P. Nita, G. Zawadzki, M. Krawiec, M. Jałochowski, *Phys. Rev. B* **2011**, *84*, 085453.
[26] M. Jałochowski, T. Kwapiński, P. Łukasik, P. Nita, M. Kopciuszyński, *J. Phys.: Condens. Matter* **2016**, *28*, 284003.
[27] C. Tegenkamp, T. Ohta, J. L. McChesney, H. Dil, E. Rotenberg, H. Pfnür, K. Horn, *Phys. Rev. Lett.* **2008**, *100*, 076802.
[28] P. Estrup, J. Morrison, *Surf. Sci.* **1964**, *2*, 465.
[29] J.-H. Lee, X.-Y. Ren, Y. Jia, J.-H. Cho, *Phys. Rev. B* **2014**, *90*, 125439, supplement.
[30] S. Modesti, L. Petaccia, G. Ceballos, I. Vobornik, G. Panaccione, G. Rossi, L. Ottaviano, R. Larciprete, S. Lizzit, A. Goldoni, *Phys. Rev. Lett.* **2007**, *98*, 126401.
[31] A. Pergament, *J. Phys.: Condens. Matter* **2003**, *15*, 3217.